HAL
open science

Water and energy transfer modeling in a permafrost-dominated, forested catchment of Central Siberia: the key role of rooting depth

Laurent Orgogozo, Anatoly S. Prokushkin, Oleg S. Pokrovsky, Christophe Grenier, Michel Quintard, Jérôme Viers, Stéphane Audry

To cite this version:

Laurent Orgogozo, Anatoly S. Prokushkin, Oleg S. Pokrovsky, Christophe Grenier, Michel Quintard, et al.. Water and energy transfer modeling in a permafrost-dominated, forested catchment of Central Siberia: the key role of rooting depth. Permafrost and Periglacial Processes, 2019, 30 (2), pp.75-89. 10.1002/ppp.1995 . hal-02538303

HAL Id: hal-02538303

https://hal.science/hal-02538303v1

Submitted on 9 Apr 2020

HAL is a multi-disciplinary open access archive for the deposit and dissemination of scientific research documents, whether they are published or not. The documents may come from teaching and research institutions in France or abroad, or from public or private research centers.

L'archive ouverte pluridisciplinaire **HAL**, est destinée au dépôt et à la diffusion de documents scientifiques de niveau recherche, publiés ou non, émanant des établissements d'enseignement et de recherche français ou étrangers, des laboratoires publics ou privés.

Open Archive Toulouse Archive Ouverte

OATAO is an open access repository that collects the work of Toulouse researchers and makes it freely available over the web where possible

This is an author's version published in: http://oatao.univ-toulouse.fr/25710

Official URL:

https://doi.org/10.1002/ppp.1995

To cite this version:

Orgogozo, Laurent and Prokushkin, Anatoly S. and Pokrovsky, Oleg S. and Grenier, Christophe and Quintard, Michel and Viers, Jérôme and Audry, Stéphane *Water and energy transfer modeling in a permafrost-dominated, forested catchment of Central Siberia: the key role of rooting depth.* (2019) Permafrost and Periglacial Processes, 30 (2). 75-89. ISSN 1045-6740.

Any correspondence concerning this service should be sent to the repository administrator: tech-oatao@listes-diff.inp-toulouse.fr

Water and energy transfer modeling in a permafrost-dominated, forested catchment of Central Siberia: The key role of rooting depth

Laurent Orgogozo[1] Anatoly S. Prokushkin[2] Oleg S. Pokrovsky[1,3]
Christophe Grenier[4] Michel Quintard[5,6] Jérôme Viers[1] Stéphane Audry[1]

[1] GET (Géosciences Environnement Toulouse), UMR 5563 CNRS/UR 234 IRD/UPS, Observatoire Midi Pyrénées, Université de Toulouse, Toulouse, France

[2] V.N. Sukachev Institute of Forest, Siberian Branch, Russian Academy of Sciences, Krasnoyarsk, Russia

[3] BIO GEO CLIM laboratory, Tomsk State University, Tomsk, Russia

[4] Laboratoire des Sciences du Climat et de l'Environnement, Université Paris Saclay, IPSL/LSCE, UMR 8212 CNRS CEA UVSQ, Orme des Merisiers, Gif sur Yvette Cedex, France

[5] Université de Toulouse, INPT, UPS, IMFT (Institut de Mécanique des Fluides de Toulouse), Toulouse, France

[6] CNRS, IMFT, Toulouse, France

Correspondence
L. Orgogozo, GET (Géosciences Environnement Toulouse), UMR 5563 CNRS/UR 234 IRD/UPS, Observatoire Midi Pyrénées, Université de Toulouse, 14 avenue Édouard Belin, 31400 Toulouse, France.
Email: laurent.orgogozo@get.omp.eu

Funding information
CALMIP supercomputing center, Grant/Award Number: p12166; Campus France, Grant/Award Number: Kolmogorov No 14.587.21.0036; Russian Science Foundation, Grant/Award Number: 18 17 00237

Abstract

To quantify the impact of evapotranspiration phenomena on active layer dynamics in a permafrost-dominated forested watershed in Central Siberia, we performed a numerical cryohydrological study of water and energy transfer using a new open source cryohydrogeology simulator, with two innovative features: spatially distributed, mechanistic handling of evapotranspiration and inclusion of a numerical tool in a high- performance computing toolbox for numerical simulation of fluid dynamics, OpenFOAM. In this region, the heterogeneity of solar exposure leads to strong contrasts in vegetation cover, which constitutes the main source of variability in hydrological conditions at the landscape scale. The uncalibrated numerical results reproduce reasonably well the measured soil temperature profiles and the dynamics of infiltrated waters revealed by previous biogeochemical studies. The impacts of thermo-hydrological processes on water fluxes from the soils to the stream are discussed through a comparison between numerical results and field data. The impact of evapotranspiration on water fluxes is studied numerically, and highlights a strong sensitivity to variability in rooting depth and corresponding evapotranspiration at slopes of different aspect in the catchment.

KEYWORDS

active layer dynamics, cryohydrogeology modeling, evapotranspiration, massively parallel computation, OpenFOAM, permafrost

1 | INTRODUCTION

Climate change is strongly pronounced at high latitudes, and has produced important changes to the distribution of permafrost,[1] which extends to approximately one-quarter the northern hemisphere landmass. Due to multiple interactions among water transfer, thermal transfer and permafrost dynamics, these changes are likely to trigger modifications in the hydrology of these regions.[2-4] Since water fluxes are the vectors of dissolved and suspended matter (including carbon) transfer along the land-to-ocean continuum, these fluxes should in turn experience major changes. To quantify such changes, accurate and quantitative modeling of the coupled thermo-hydrological behavior of permafrost catchments is needed.

Weathering of rocks is among the most important processes involved in the transfer of dissolved and suspended material in continental surfaces. Modeling of weathering permafrost-affected areas is thus key in the prediction of future global carbon dynamics.[5] To develop predictive modeling of weathering in boreal areas, we need relevant thermo-hydrological input data that accurately describe the seasonal dynamics of infiltrated waters, such as regarding drainage, temperature, water content and water state along soil profiles, and water residence time within the slopes, because infiltrating water is

both the agent of chemical weathering and the vector of riverine fluxes.[6] Also of importance for the interaction between permafrost dynamics and the carbon cycle is the fate of soil organic carbon during permafrost thawing[7,8] and thermokarst genesis.[9-11] Modeling of some of these phenomena has already been undertaken at the continental scale,[12] but the highly sensitive nature of the results to hydrological regime[13] illustrates the need for careful assessments of the thermo-hydrological processes involved. Mechanistic modeling studies at the scale of individual catchments are required.

For the study of biogeochemical dynamics of boreal areas, cryohydrogeological modeling, which deals with coupled hydrological and thermal transfers within variably saturated porous media (e.g. soils or geological bodies) with freeze–thaw of the pore water, is essential. Numerical resolution of the governing equations for the associated systems is difficult, due to numerous and strong non-linearities and strong couplings between the factors involved. Numerous studies have therefore investigated this subject, from the early 1970s[14] until the present.[15,16] It is now recognized as a hot topic in permafrost studies.[4] As emphasized above, cryohydrogeological modeling is vital for biogeochemical studies of boreal areas, but there are many other potential fields of application of cryohydrogeological models, such as geotechnics,[17] long-term storage of nuclear waste,[18-20] water resources in cold regions,[21,22] thermal transfer around pipelines in cold regions,[23,24] infrastructure stability[25-27] and geothermics in cold regions.[28]

One of the major difficulties in cryohydrogeological modeling lies in the fine temporal and spatial resolution needed to numerically solve the equations involved.[29] Such high-resolution simulations require large and high-performance computational resources,[30] as now acknowledged for the whole field of hydrological modeling.[31] For these reasons, massively parallel simulation tools have been developed in recent years.[32,33] Indeed, in the biogeochemical applications discussed above, large temporal and spatial scales may be encountered (typically tens of years and of square kilometers in the study of climate at the watershed scale), which requires high-performance computing techniques.

In this work, we developed a dedicated cryohydrogeology numerical simulator in the framework of OpenFOAM (www.openfoam.com), an open source toolbox for computational fluid dynamics widely used in various industrial and scientific applications. One of the main strengths of OpenFOAM is its ability to use massively parallel computing techniques efficiently. For example, the parallel performance of OpenFOAM has been assessed in some geosciences applications.[34,35] As discussed by Orgogozo *et al*.,[35] working in an open source generalist framework such as OpenFOAM benefits from community-driven developments by large groups of users and developers. In this way, many state-of-the-art pre-processing, solving and post-processing tools that are continuously developed within the OpenFOAM community can be applied for various specific problems.[36,37] These two aspects, namely good parallel performance and the integration in an open source generalist framework, motivated our choice of developing permaFOAM, an OpenFOAM solver for cryohydrogeology. The permaFOAM numerical approach was successfully validated recently from two bidimensional and fully saturated test cases within a benchmark of 13 codes.[38]

Here we focus on the modeling of water and energy transfer in an experimental watershed in Central Siberia, located within the Siberian basaltic trap province and covered by larch forests. The remoteness, vast extent (~1.5 million km^2) and the lithological and landscape homogeneity of this area make it an ideal region for studying chemical weathering processes and river export fluxes in a permafrost terrain.[39-42] The main spatial variability in these landscapes relates to the south- or north-facing aspects of the slopes. The Kulingdakan watershed is a small (~40 km^2) catchment in this region, and it has been monitored for more than a decade in order to characterize its biogeochemical dynamics.[43,44] Cryohydrogeological modeling of this catchment is thus of great interest, because it can both benefit from the already acquired biogeochemical data and help to further interpret the available data.

The heterogeneity in solar radiation received by the different aspect slopes leads to highly contrasted thermo-hydrological conditions in the considered catchment, as has been observed in other permafrost-dominated environments.[45,46] In the Kulingdakan catchment, variability in evapotranspiration in relation to solar exposure has been identified as a key control on active layer dynamics.[47] Here we investigated this variability through mechanistic numerical modeling of the active layer dynamics of the slopes of the watershed, using a distributed, processes-based estimator of the evapotranspiration flux, which is an adaptation of Orgogozo[48] to permafrost environments. For this we compared the numerical results of a coupled thermo-hydrological mechanistic modeling with field measurements of temperature profiles in both slopes with a southern aspect (SAS) and northern aspect (NAS). Quantitative estimates of the water fluxes obtained from numerical results allow us to discuss the different terms of the hydrological budget based on field data acquired on water and heat transfer in the Kulingdakan watershed, with a focus on seasonal dynamics of infiltrated waters. The sensitivity of evapotranspiration fluxes to the spatial variability in tree morphology (rooting depth) inherited from the spatial variability of solar exposure was also investigated by means of numerical experiments that compute evapotranspiration fluxes for various rooting depths. The results of this study will be useful for prediction of water fluxes and pathways responsible for changes of environmental conditions such as active layer thickness and vegetation dynamics.

2 | MATERIAL AND METHODS

In this section we present the numerical permaFOAM tool, discuss the studied site and the associated data set, together with the set-up of the proposed modeling.

2.1 | The permaFOAM simulator

2.1.1 | Considered governing equations

The cryohydrogeological numerical model permaFOAM deals with coupled water and thermal transfer within three-dimensional (3D) heterogeneous, variably saturated porous media, with freeze–thaw of the pore water. The media considered may be four-phase with a solid

phase, a liquid water phase, an ice phase and an air phase. Our goal was to find a trade-off between the accuracy of the description of physical phenomena and the ability to deal with large spatial and temporal scales, which implies fast and robust computation. The variations in water density with respect to its state (liquid/frozen) and temperature are not considered, and the solid matrix is non-deformable. Thus, soil mechanics and cryoturbations[49] are not taken into account, and nor is water natural convection due to density-driven flow and cryosuction. Cryosuction, which is responsible for liquid water flux toward freezing fronts,[50,51] is closely related to cryo-mechanical processes, jointly with the ice volumetric expansion.[52] The freezing point depression effect has also not been taken in consideration, and because salt concentrations in these soil pore waters are low, the maximum temperature at which the ice can exist is considered to be constant. We assumed the existence of a local thermal equilibrium, which is classical in this field.[4] Finally, we consider a Richards formulation to describe the flow of water, and we do not take into account advective transport of heat and water vapor by air.[53] These simplifying assumptions lead to a system of equations of classical form[15,16] with two coupled equations.

First, a modified Richards equation with a source term accounting for actual evapotranspiration governs the total mass balance for water and ice (see Supporting Information Appendix S1 for the fully detailed equation system with complete nomenclature):

$$C_H(h)\frac{\partial h}{\partial t} \quad \nabla.(K_H(h,\ T)\nabla(h+z)) + Q_{AET}(h,\ T) \tag{1}$$

The left-hand side of Equation (1) is the mass storage term, whereas the first term on the right is the divergence of the Darcy flux and the second term is a sink term for evapotranspiration. From this the filtration velocity field is computed on the basis of the field of pressure head (the primary variable of Equation (1)), by a generalized Darcy's law:

$$\mathbf{V}(h,T) \quad -K_H(h,T)\nabla(h+z) \tag{2}$$

Second, a macro-scale heat transfer equation for a porous medium with a term of latent heat exchange governs thermal transfer:

$$\frac{\partial\left(\left(C_{T,eq}(h,T) + L\frac{\partial\theta_{ice}(h,T)}{\partial T}\right)T\right)}{\partial t} + \nabla.\left(\mathbf{V}(h,T)C_{T,liquid}T\right) = \nabla.\left(K_{T,eq}(h,T)\nabla T\right) \tag{3}$$

The first term in the left-hand side of Equation (3) is the heat storage term (which includes heat stored in latent form) and the second term is the advective flux term, which includes the filtration velocity computed in Equation (2). The right-hand side of Equation (3) represents the conductive flux. Apparent hydraulic conductivity in a variably saturated and variably frozen porous medium is here given by:

$$K_H(h,T) \quad K_s K_{rel}(h) K_{freezing}(T) \tag{4}$$

Liquid water/ice equilibrium in the soil is described through an empirical soil freezing characteristic (SFC) function[20] as:

$$\theta_{liquid}(h,T) \quad \begin{cases} \theta(h) & \text{if } T > T_{freeze} \\ \theta_r + (\theta(h) - \theta_r)\exp\left(-((T - T_{freeze})/w)^2\right) & \text{if } T \le T_{freeze} \end{cases} \tag{5}$$

and the ice volume fraction is calculated from the total water volume fraction as:

TABLE 1 Physical meanings and units of the symbols used in Equations (1)–(6)

Parameter	Definition	Units
t	Time	[s]
z	Upward vertical coordinate	[m]
h	Total water pressure head	[m]
T	Temperature	[K]
C_H	Capillary capacity	[m ^{1}]
K_H	Apparent hydraulic conductivity of the variably saturated and variably frozen porous medium	[m s ^{1}]
Q_{AET}	Volumetric actual evapotranspiration rate	[s ^{1}] (~[m^3 water m ^{3} soil s ^{1}])
$C_{T,\ eq}$	Apparent heat capacity	[J m ^{3} °C ^{1}] (~ [kg m ^{1} s ^{2} K ^{1}])
L	Latent heat of fusion of ice	[J m ^{3}] (~ [kg ^{3}m 1 s ^{2}])
θ_{ice}	Volumetric ice content	[–]
θ_{liquid}	Volumetric liquid water content	[–]
θ	Total volumetric water content	[–]
θ_r	Residual liquid water content	[–]
$\mathbf{V}$	Filtration velocity	[m s ^{1}]
$C_{T,\ liquid}$	Heat capacity of liquid water	[J m ^{3} °C ^{1}] (~ [kg m ^{1} s ^{2} K ^{1}])
$K_{T,\ eq}$	Apparent thermal conductivity	[W m ^{1} °C ^{1}] (~ [kg m s ^{3} K ^{1}])
K_s	Saturated unfrozen hydraulic conductivity	[m s ^{1}]
K_{rel}	Relative hydraulic conductivity of the unfrozen variably saturated porous medium	[–]
$K_{freezing}$	Relative hydraulic conductivity of the saturated variably frozen porous medium	[–]
T_{freeze}	Maximum temperature at which ice may exist	[°C] (~ [K])
w	Scaling parameter of the SFC function	[°C] (~ [K])

$$\theta_{ice}(h,T) \quad \theta(h) - \theta_{liquid}(h,T) \tag{6}$$

The physical meanings and the units of the symbols used in the equations are listed in Table 1.

Classical parameterizations are considered for the coefficients of these equations, and are described in details in Appendix S1. We use a Mualem–van Genuchten approach[54] for the retention curve, the capillary capacity C_H and the relative hydraulic conductivity with respect to saturation K_{rel} and an empirical power law parameterization for relative hydraulic conductivity with respect to freezing of the porous medium, $K_{freezing}$.[19,55] Note that the primary variable of the considered generalized Richards equation (Equation (1)) is a pressure head h defined for the total water phase (liquid + ice). A similar approach is used by Guymon and Luthin[14] and Weismüller *et al.*[56] Obstruction of the porous medium by freezing is taken into account through a heuristic approach by the multiplication of the classical apparent unfrozen hydraulic conductivity K_sK_{rel} by $K_{freezing}$ (Equation (4)). The estimator used for the actual evapotranspiration Q_{AET} is based on the potential evapotranspiration and on the geometry of the evapotranspiration zone.[48] The approach adopted here allows us to consider actual evapotranspiration whenever and wherever there is enough water in the soil of the evapotranspiration zone to satisfy potential evapotranspiration. The only modification in permaFOAM compared to the implementation of Orgogozo[48] is the use of volumetric liquid water content instead of volumetric total water content in computing the actual evapotranspiration sink term, in order to take into account freezing of the water phase in the soil pore space of the root zone. We adopt a simple mixture model for evaluation of the apparent thermal conductivity of the variably saturated and variably frozen porous medium, $K_{T,\ eq}$.[57] We do not take into account the thermal dispersion in soils, which is generally small compared to thermal diffusion.[15] The apparent heat capacity of the variably saturated and variably frozen porous medium $C_{T,\ eq}$ is classically evaluated with an arithmetic mean of the heat capacity of each phase.[58] Note here that the air phase is taken into account in computation of the effective thermal properties of the four-phase medium considered, although Richards assumptions lead to a formulation of water transfer in variably saturated porous media in which the air phase does not appear explicitly. Latent heat exchanges are handled with a simple apparent specific heat method.[19,59]

2.1.2 | Numerical methods

We use two Picard loops to deal with non-linearities, one for Richards Equation (1) and one for the thermal Equation (3), and a sequential operator splitting approach to deal with the links between these two equations. Thus at each time step, the water balance (Equation (1)) is solved first, with a Picard loop to deal with its non-linearities, and the thermal equation (Equation (3)) is then solved with updated effective properties for the porous medium and water fluxes, and also with its own Picard loop. Since permaFOAM is based on OpenFOAM (www.openfoam.com),[60] the partial differential equations are solved in three dimensions by a finite volume method. An empirically based automatic adaptive time step strategy is implemented, based on convergences of the two Picard loops.[61] Additional numerical details (including validations) regarding resolution of the Richard's equation (Equation (1)) with OpenFOAM are given in Orgogozo *et al.*,[35] and the approaches adopted here to deal with the thermal equation (Equation (3)) are very similar. The OpenFOAM solver permaFOAM implemented as described above has been successfully validated in saturated conditions by comparison with 1D benchmark test cases available in the literature,[55,62] and with 2D test cases in the framework of the international benchmark InterFrost.[38] Further validation and details of permaFOAM are given in Data S1 and Data S2, respectively.

2.2 | Study site, field data set and estimations of thermo-hydrological forcings

In this section we describe the thermo-hydrological setting of the Kulingdakan watershed and how we used the acquired data to estimate the fluxes of water and heat to the soil of the catchment slopes.

2.2.1 | The experimental watershed of Kulingdakan

The Kulingdakan watershed is situated at 64°17′N, 100°11′E, about 5 km north-east of Tura, in a continuous permafrost area. It has a roughly rectangular shape (~8 km E–W, ~5 km N–S), and the stream is oriented from east to west, and as such it may be divided into two, roughly equal areas differentiated solely based on aspect, one with a northern aspect and the other with a southern aspect. The average incline of the watershed slopes is 20%, and the altitude difference between the outlet and the highest point is about 500 m.[47] No taliks are known in the Kulingdakan watershed,[42] so we can make the hydrological balance of the watershed on the basis of meteorological water input only. This allows us to make a simplified representation of the watershed by two 2D transects (Figure 1), each representing a side of the watershed, either for NAS or for SAS.

Structural differences in the soils of each side have important controls on their thermo-hydrological regimes,[64] and a pedological survey of the Kulingdakan watershed allowed us to assess this structural variability.[63] The soils of the watershed consist of two horizons: a mineral horizon (mainly rocky/gravely loam) resulting from weathering of underlying basalts and, overlying this, an organic horizon composed of larch, moss and dwarf shrub litter. These soils are topped by a thick insulating layer of mosses and lichens. The thicknesses of these layers vary between NAS to SAS. For example, organic soils in SAS have an average thickness of 8 cm, while in NAS this is 12 cm. The average thickness of the moss and lichen layer ranges from 6.5 cm in SAS to 13 cm in NAS. Vegetation cover varies strongly between SAS and NAS, both in terms of aerial biomass (SAS: 3.02 kgC/m^2; NAS: 1.53 kgC/m^2) and in terms of leaf area index (SAS: 0.69 m^2/m^2; NAS: 0.2 m^2/m^2). Rooting depth also differs strongly between slopes (depth into the mineral horizon: 60 cm in SAS, 10 cm in NAS), although root biomass is fairly similar (SAS: 0.44 kgC/m^2; NAS: 0.55 kgC/m^2). This high morphological variability of the tree stands between slopes stems from the fact that better insolation in SAS leads to fewer but higher, larger and healthier trees than in NAS (see Figure 1). Additional details on the vegetation cover of this region are provided by Prokushkin *et al.*[65]

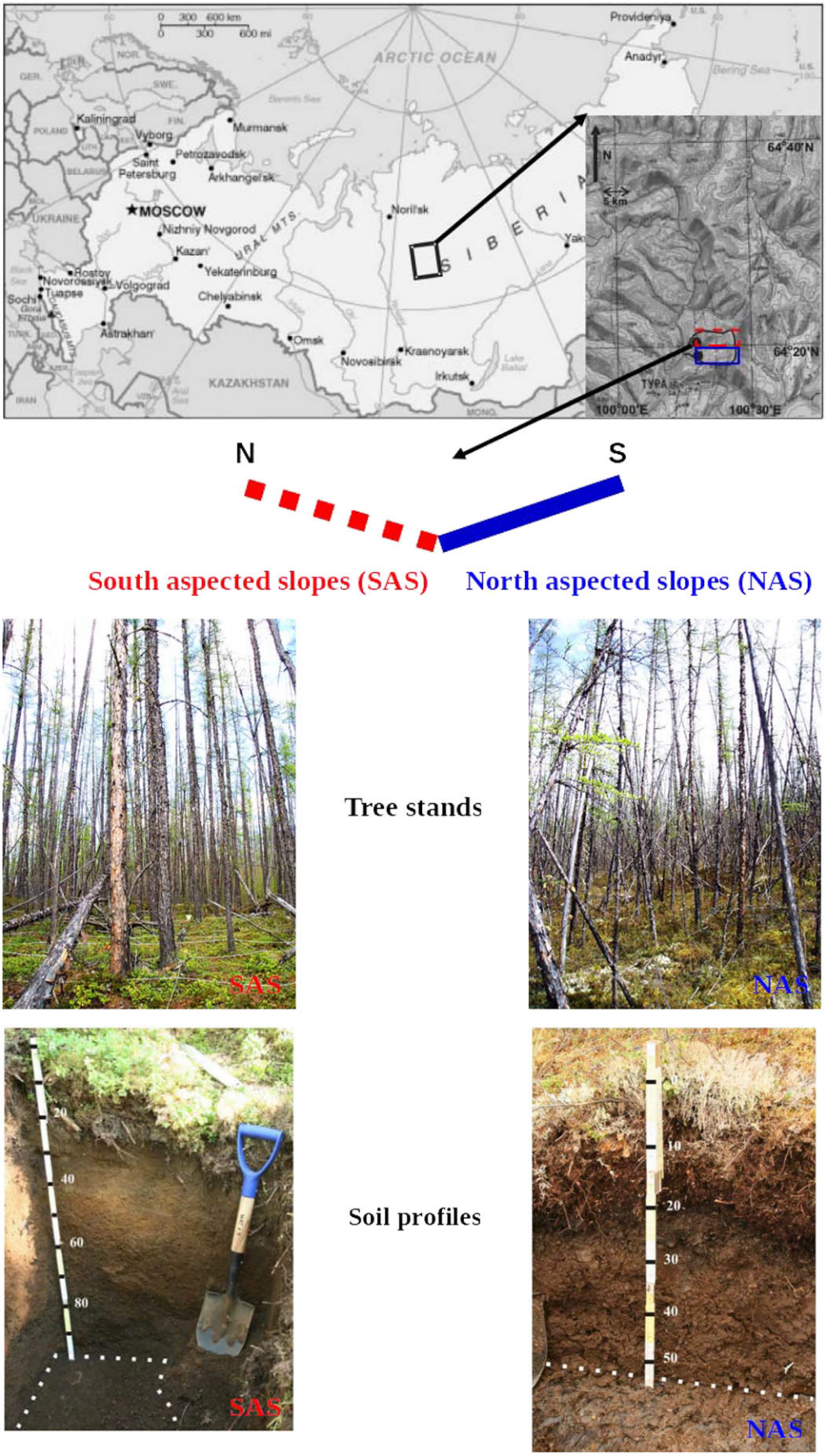

FIGURE 1 Top: location, orientation and shape of the Kulingdakan watershed (modified from Prokushkin *et al.*[43]), and scheme of simplified 2D description of the watershed; middle: photos of the contrasted tree stands in both slopes; bottom: photos of the pedological profiles at the two sites of monitoring of the temperature profiles (modified from Gentsch[63]) [Colour figure can be viewed at wileyonlinelibrary.com]

2.2.2 | Monitoring of soil thermal state and of meteorological conditions

To characterize the dynamics of the active layers of this watershed, time series of temperature profiles were acquired daily using TR-52 sensors (T&D Corp., Japan) both on SAS and NAS (Figure 1) at different depths (top of the moss layer, top of the organic layer, top of the mineral horizon and 10 cm and 20 cm depth within it) and at an altitude of about 100 m above the outlet of the watershed. These time series of soil temperature profiles, along with meteorological data acquired at Tura (daily measurements), were processed to produce a multi-annual average data set (time window: from 2003 to 2012) of monthly soil temperatures and monthly climatic forcing data (liquid rain water input and potential evapotranspiration) to study thermo-hydrological dynamics that are representative of current conditions. We consider monthly averaged data because we are interested in transfer within the soils, which shows smooth variations compared to surface transfer. Thus, the results here are presented at a monthly temporal resolution, and all analyses were performed at this resolution. Note that modeling the transfer in the watershed with a higher temporal resolution would require us to consider (i) complete surface runoff processes, (ii) transfers within the highly conductive moss layer and (iii) snowpack dynamics. These issues were beyond the scope of this paper. This data set of multi-annual averages of monthly values is presented in Figure 2, which shows the forcings used as input data for the modeling (i.e. the data used to build boundary conditions and potential evapotranspiration fields).

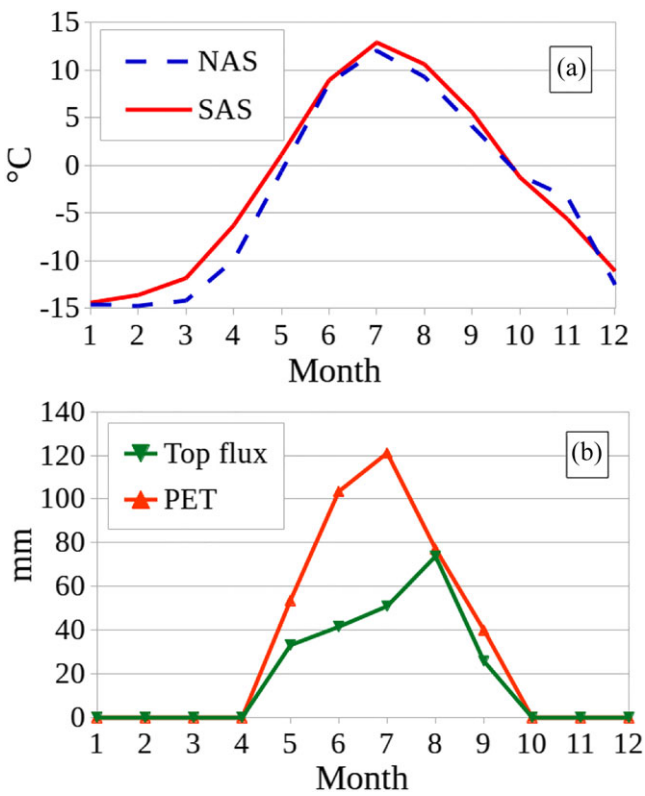

FIGURE 2 Forcings used as input data for the thermo-hydrological modeling (monthly averages). –(a) Temperature at the top of the organic layer for each aspect. –(b) Estimates of the liquid water flux at the top of the organic layer and of potential evapotranspiration (PET), both of which are similar for NAS and SAS [Colour figure can be viewed at wileyonlinelibrary.com]

Figure 2(a) presents the temperatures at the top of the organic layer rather than the surface temperatures (i.e. temperatures at the top of the moss layer) for both NAS and SAS, in order to have thermal input data that characterize the soils, encompassing the effects of different radiation dynamics and thermal transfers within the snow packs and the moss layers for each slope. In Figure 2(b), the liquid water flux at the top of the organic layer is estimated as the monthly total of the liquid rain (i.e. interception losses are neglected) when the monthly mean temperature at the top of the moss layer (data not shown) is above 0°C. This liquid water flux at the top of the soils is not total rain nor infiltration flux, but only the part of the rain that falls in a liquid state when the frozen ground starts to thaw, and which thus may infiltrate into the soil, depending on the hydraulic status of the soil in question. The part of this top water flux that actually infiltrates is computed depending on the saturation status of each mesh cell of the top boundary at each time step. When the snow pack melts during spring flood, we assume that the entire flux of snowmelt goes directly to the river through surface runoff or flows within the moss layer. This seems reasonable since the spring flood is fast (about 2 weeks at the end of May to beginning of June) and occurs when the organic (top) layer of the soils is still frozen. Indeed, hydraulic conductivity of the frozen organic layer is very low while that of the saturated moss is very high,[66,67] so the lateral drainage of snowmelt water through the thick moss layer is likely to be fast compared to the infiltration rate within the still frozen organic layer. However, the snowpack distribution and its rate of melting are controlled by complex phenomena that depend on, for example, land cover, insolation and snow depth,[68,69] are of which all variable between NAS and SAS. Moreover, there are field observations of snowmelt waters that infiltrate the soil of some permafrost-affected areas at the beginning of the spring flood, due for example to frost cracks.[70] Although these points were beyond the scope of this study, they merit further investigation to take into account the impact of spring flood on active layer dynamics.

2.2.3 | Estimation of potential evapotranspiration

Here, potential evapotranspiration (Figure 2b) has been computed using the Hamon formula,[71,72] which has already been used in studies of forested boreal areas (spruce/moss boreal forest):[73]

$$PET_d = \begin{cases} 218,527\dfrac{L_d}{T_{air}+273,3}\exp\left(17,26939\dfrac{T_{air}}{T_{air}+273,3}\right) & \text{if } T_{air} > 0 \\ 0 & \text{if } T_{air} \leq 0 \end{cases} \quad (7)$$

In Equation (7), PET_d is daily potential evapotranspiration [mm/d], L_d is day length which is the time from sunrise to sunset in multiples of 12 hours [12 h ^{1}] (which depends mainly on latitude – data not shown) and T_{air} is daily mean air temperature [°C] (data not shown).

This formula takes into account the temporal but not spatial variations of solar insolation, but not variations in land cover. Thus, these two effects are taken into account only in the computation of actual evapotranspiration, through the differences in thermal and

hydrological status in each slope, and through the prescribed geometry of the evapotranspiration zone. This means that potential evapotranspiration in NAS and in SAS is the same (although actual evapotranspiration in NAS and SAS is different, see section 2.3.3).

2.3 | Modelling set up

2.3.1 | Geometry and properties of the computational domains

Both NAS and SAS slopes of the watershed are represented by a 2D transect of 2.5 km length and 20% incline, corresponding to the average slope in the watershed. This means that we neglect the morphological variability of the watershed along the stream and lateral flux along the direction of the stream axis, and that the small tributaries of the main stream are not considered. The thickness of these transects (from the top of the soil to the bottom of the modeling domain) is fixed at 10 m, as this is a common depth of a year-round stable temperature in boreal environments.[74] We model only the soil horizons (organic and mineral), without considering the water and energy balances at the surface of the moss layer or the transfers within it. This is justified by the availability of temperature data at the interface between the moss layer and the organic layer and by fast water transfer within the moss layer. Thus, we have a simple heterogeneous medium with two layers: the upper organic layer and the underlying mineral horizon, in which we do not differentiate between the secondary clays, weathered basalt and fresh bedrock. The hydrodynamic and thermal properties of these two components of the Kulingdakan slopes are taken from the literature,[14,75,76] without any calibration and fitting, and are presented in detail in Appendix S2.

2.3.2 | Boundary conditions

The boundary conditions considered, as well as the geometric features of the modeling domains, are summarized in Figure 3.

For the thermal equation (Equation (2)), we consider a monthly fixed temperature at the top of the domain, equal to the measured temperature at the top of the organic layer (see Figure 2a). In this way, the thermal top boundary conditions for our simulations encompass the effects of radiation dynamics and thermal transfer within the snow pack and the moss layer, and as a consequence we do not need to model these complex processes. The bottom boundary flux condition is fixed, with a flux equal to the geothermal flux in the region of the Putorana plateau (0.038 Wm ^{1}).[77] The up- and down slope vertical boundary conditions are not thermal gradient boundary conditions.

From the point of view of hydrology, we impose a boundary condition of fixed monthly flux equal to the liquid water flux at the top of the organic layer (see Figure 2b) if the upper boundary is unsaturated. In the case of a saturated upper boundary, the infiltration of water is impossible, and we then switch to an atmospheric pressure head boundary condition, so that we can model exfiltration (i.e. flux of water from the soil due to subsurface flow). As such, there is no direct and complete modeling of surface runoff, because we are mainly interested in the infiltration of water into the soil necessary for modeling of future weathering. A fully coupled surface flow – subsurface flow approach would be needed to quantify total stream flow, but this complex problem[33,78] is beyond the scope of this study. The bottom boundary condition is a zero water flux, as the rock is completely frozen year round at 10 m depth (and even much shallower) and because there are no taliks in the watershed. The downslope boundary condition is hydrostatic, taking into account

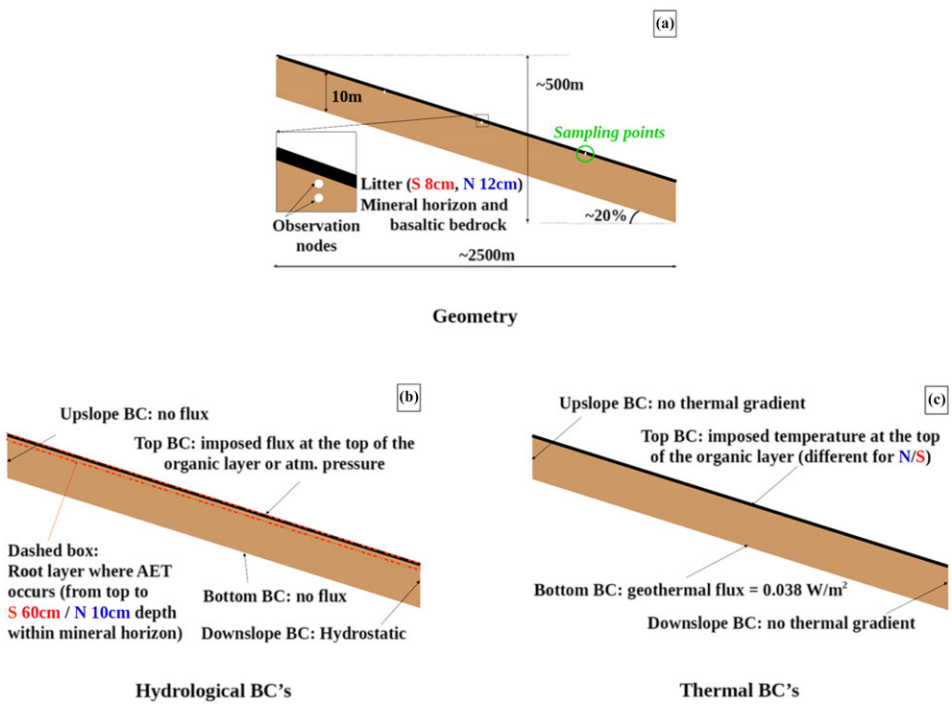

FIGURE 3 Domains of modeling and boundary conditions. –(a) Description of the domains. –(b) Hydrological boundary conditions. –(c) Thermal boundary conditions. In italic green in (a) is the location of the numerical sampling points considered as equivalent to the field measurement points [Colour figure can be viewed at wileyonlinelibrary.com]

the presence of the stream. Finally, the upslope hydrological boundary condition is no water flux (i.e. symmetry).

2.3.3 | Efficiency of potential evapotranspiration: field of actual evapotranspiration

Because we are considering a forested and cold environment, we assume that the evapotranspiration flux is due mainly to transpiration by vegetation, and we neglect physical evaporation. As a consequence, we identify the evapotranspiration zone and the root zone, whose thickness is different between NAS and SAS. Water uptake via evapotranspiration is then assumed to occur only in the root layer, which is developed at up to 60 cm depth within the mineral horizon in SAS and up to 10 cm depth within the mineral horizon in NAS.[79] Root layer thickness is then the only parameter that is considered in order to take into account the variability of vegetation morphology between SAS and NAS in the computation of evapotranspiration fluxes. Actual evapotranspiration water uptake is computed for both slopes at each point of this layer and at each time step on the basis of (i) potential evapotranspiration and (ii) the thermo-hydrological status of the soil, given that evapotranspiration uptake of soil water can occur only in the parts of the root layer in which there is available liquid water (i.e. where pressure head is greater than the wilting point[48] and where temperature is above 0°C). The differences in actual evapotranspiration fluxes between NAS and SAS stem from different thermal forcings at the top of the soil (see Figure 2a) as well as different tree cover (and thus different rooting depths).

2.3.4 | Simulated point evolutions

To sample the inner fields along the computations, observation nodes that record the temperature and water content at each time step of the computations have been implemented at 10 cm depth and 20 cm depth within the mineral horizon at five points regularly disposed along the slopes (see Figure 3a). The second points from the bottom of the slopes (reported in italic green in Figure 3a) are at a position close to thatof the measurement sites in the field, and thus they are used for comparison between the numerical results and observations. Having points regularly disposed along the slopes allowed us to investigate the variability of the thermo-hydrological regime along the slope.

2.3.5 | Initial conditions and spin up

The initial conditions have been estimated in the following way. First, an estimate of the spatially averaged mean annual temperature in each slope is obtained by a steady-state computation of purely diffusive thermal flux in water-saturated slopes. These spatially averaged mean annual temperatures are then used as the values of uniform initial temperature fields for a first year of transient modeling of the coupled thermo-hydrological behavior of the total domains. The initial water pressure head field was fixed to a hydrostatic field in the mineral soil (i.e. fully saturated mineral horizon) and to the field capacity pressure head within the organic layer. The temperature and pressure head fields at the end of the first year of transient modeling are then used as the initial conditions for a second year of transient modeling, and so on until a dynamic equilibrium was reached. We stop the cycling process when stabilization is reached for the temperature field (difference between year n and year $n + 1$ at the same dates at the points of sampling lower than 0.1°C), the total water content field (difference between year n and year $n + 1$ at the same dates at the points of sampling lower than 0.01%) and the water fluxes across the upper boundary (relative difference between year n and year $n + 1$ at the same dates lower than 5%). The results of the previous year of cycling were considered as the steady-state thermo-hydrological dynamic regime in each slope under current climatic conditions, and these results are presented below.

2.3.6 | Numerical discretizations and precision of the computations

The 2D domains are discretized by vertically graded meshes of about 2.5 million cells (cells of thicknesses ranging from 5×10^{-3} m at the top of the domain to 0.2 m at the bottom; constant width of 0.2 m; 200 cells over the vertical axis; about 12,500 cells over the horizontal axis). The requested precisions of the linear solvers and of the linearization loops varied with the month and slope, because thermo-hydrological regimes were strongly different. They have been established through a careful study of convergence, for which we have compared the actual results with those obtained with refined computations with 10 million mesh cells, 100 times higher resolutions for linear solvers, 10 times higher resolutions for linearization loops, and 10 times smaller maximum time steps. The differences between the actual and refined computations for the temperature and the total water content fields were evaluated at all the numerical probes, and were lower than 0.05°C for the temperature field and lower than 0.001 for the total water content field. Convergence was less satisfactory for water fluxes across the upper boundary, with an upper bound of 33% in relative difference between the actual and refined computations.

2.3.7 | Computational resources

The computations were made based on requests of 20–500 cores (processors: IntelIVYBRIDGE 2.8 GHz 10-cores) on the CALMIP cluster EOS (www.calmip.univ-toulouse.fr). The good parallel capabilities of permaFOAM were necessary to achieve computations with such unprecedented spatio-temporal resolutions. A brief assessment of the parallel performances experienced with permaFOAM on the EOS cluster is given in Appendix S3.

3 | RESULTS

3.1 | Temperature and water contents within the active layer

A comparison between numerical results and field measurements for the temperature in the mineral soils of both SAS and NAS of the Kulingdakan watershed demonstrated reasonable agreement (Figure 4). These values

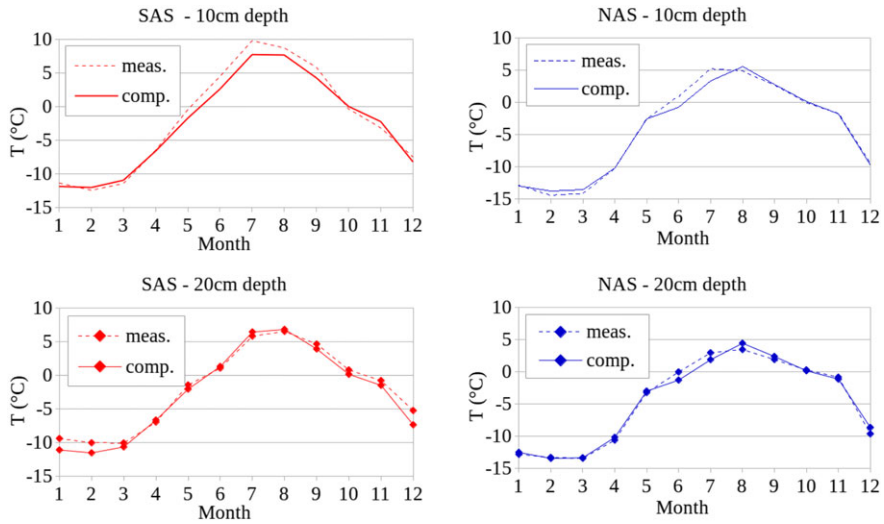

FIGURE 4 Measured and computed temperatures in SAS and NAS at 10 cm and 20 cm depth within the mineral horizon, at the point of field sampling [Colour figure can be viewed at wileyonlinelibrary.com]

(either computed or measured) are those at the points of sampling (Figure 3). Only comparisons between monthly averaged numerical results and monthly averaged field observations were possible, because the intrinsic simplifications of the modeled domains and phenomena prevented us from making analysis at a finer time scale. A monthly time scale analysis was also coherent with our main objective, i.e. the study of seasonal dynamics of infiltrated waters.

As expected, SAS are generally warmer than NAS. Soil temperatures exceed 0°C about 1 month earlier in SAS than in NAS. One can also see the effect of depth on these temperatures, with smaller amplitudes of seasonal variations with increasing depth. These features are well reproduced by the numerical modeling. Mean absolute differences are below 1°C for both slopes, with root mean square error between measured and computed values of 0.74°C in NAS and 1.07°C in SAS. Variations of the thermal regimes observed in NAS and SAS are closely related to the variation of hydraulic states between them.

The computed seasonal variations of total water, liquid water and ice contents at the sampling points in both slopes (Figure 5) demonstrated that, as expected, the SAS are dryer and thaw earlier than the NAS. These hydraulic patterns correlate well with the thermal dynamics observed above.

Although the comparison between numerical results and field measurements has only been done on point values, bidimensional variability has been detected from the simulations. Thus, temperature profiles along the slope at 20 cm depth in the mineral soil in both SAS and NAS are dependent on distance to the stream (Figure 6).

There are strong differences between the top temperature and the near stream temperature both in SAS (3.5°C) and NAS (4.7°C). Nevertheless, an area of low variability may be observed far from the boundaries. The difference in temperature at the bottom of the slopes between NAS and SAS is mainly a numerical artefact due to the separate modeling of each slope. A more realistic geometrical description such as a V-shaped section that represent both slopes at the same time would enforce temperature continuity at the bottom of the slopes. Note, however, that a flat riparian area up to 100 m wide exists around the stream at the bottom of the slopes, which gives some consistency to the separate slopes approach adopted here.

3.2 | Water fluxes from SAS and NAS

3.2.1 | Evapotranspiration

The major flux of water from the soils is evapotranspiration flux. Since the Kulingdakan watershed is almost completely forested and the climate is cold (mean annual air temperature: −8°C), the main component of evapotranspiration is transpiration by trees. Consequently, the actual evapotranspiration should be strongly impacted by tree morphology, for instance by rooting depth, which is highly variable between NAS and SAS.[79] To analyse the impact of rooting depth on water fluxes, numerical experiments were performed for different thicknesses of the root layers. The results presented in Figures 4, 5 and 6 were obtained by considering in the computations the measured rooting depth in NAS (10 cm within the mineral horizon) and SAS (60 cm within the mineral horizon, about the mean value observed in boreal forests[80]). This set of computations and results are termed the Actual Conditions case (AC case) in our subsequent discussions. An additional set of computations was then done in accordance with

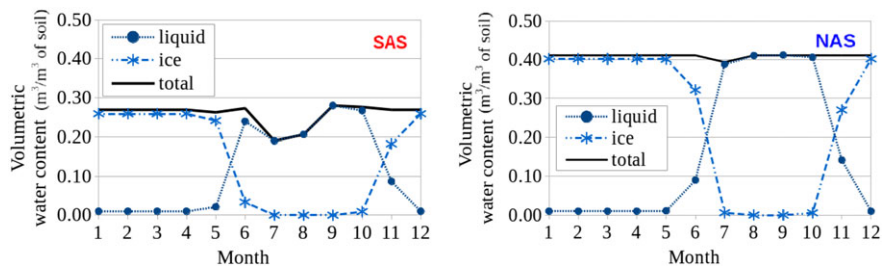

FIGURE 5 Computed seasonal evolution of liquid, ice and total water contents at 20 cm depth within the mineral horizon in NAS and SAS [Colour figure can be viewed at wileyonlinelibrary.com]

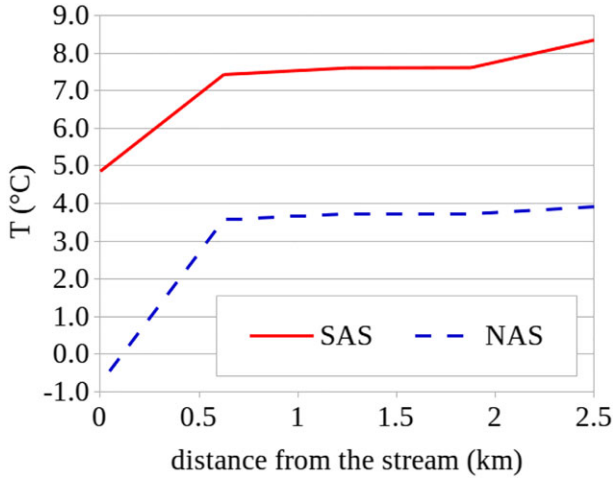

FIGURE 6 Computed temperatures along slopes (20 cm depth within the mineral horizon) in July in SAS and NAS [Colour figure can be viewed at wileyonlinelibrary.com]

this previous one, except that a constant 1 m rooting depth (equal to the global mean value[80]) was considered in both NAS and SAS. This second set of computations and results is designated the Artificially Deeper Roots case (ADR case) below. Comparative analysis of these two sets of computations allowed us to investigate the impact of rooting depth on water fluxes in boreal forested environments. Figure 7 provides computed actual evapotranspiration for both slopes, for the two sets of numerical computations: actual results with the observed rooting depths (AC case), and numerical experiment results with a constant 1-m-thick root zone (ADR case).

Strongly contrasted behaviors occur in the two sets of computations. The AC case exhibits large differences in actual evapotranspiration between SAS and NAS, due to a faster and stronger increase of active layer thickness in SAS than in NAS. The computed maximum (end of July) active layer thickness is 1.41 m in SAS and 0.62 m in NAS. Note that these numerical results are in good agreement with the field data, which report a maximum active layer thickness of 1.22 m in SAS and 0.58 m in NAS.[63] In the ADR case, the maximum active layer thicknesses are almost equal (1.1 m in SAS and 0.9 m in NAS), leading to smaller differences in actual evapotranspiration between slopes than in the AC case. The resulting differences in hydraulic regimes between the two set of numerical computations are particularly strong in NAS, which are year-round water-saturated in the AC case but experience a drying period (i.e. time with actual evapotranspiration higher than rain) in summer in the ADR case. This indicates that rooting depth exerts strong controls on evapotranspiration fluxes in such forested, permafrost-dominated areas, with important impacts on the thermal and hydrological states in the uppermost layers of the soil. Note that the field observations of hydromorphism in NAS are in good agreement with the AC case results.

3.2.2 | Exfiltration

The other water flux from the soils of the slopes is exfiltration, i.e. the flux of subsurface water coming from the soil due to subsurface flow. Our computations show that exfiltration flux represents less than 1% of the evapotranspiration flux. The explanation for this huge difference between evapotranspiration and exfiltration fluxes may be that most infiltrated waters are evapotranspirated before reaching the permafrost table, above which they should flow to feed the exfiltration flux coming from the soil through the top surface of the active layer at the bottom of the slopes. Nevertheless, exfiltration is an important flux when considering weathering processes, because it exports matter directly from the soil to the stream. Note that in this analysis we do not take into account

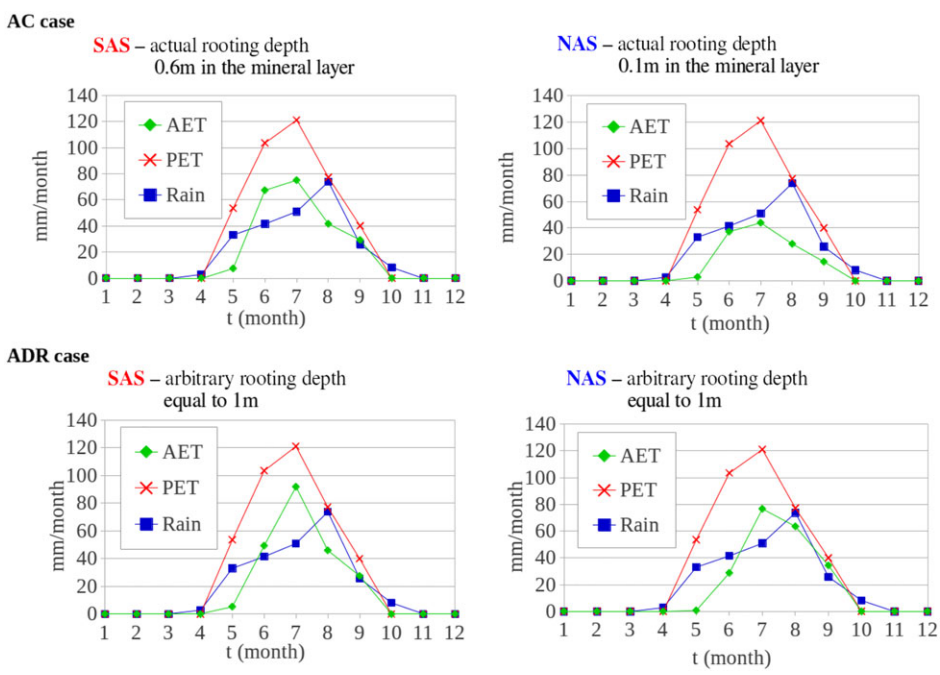

FIGURE 7 Computed seasonal evolution of actual evapotranspiration (AET) and input data of top water flux (Rain) and of potential evapotranspiration (PET) within NAS and SAS. Top, AC case: results obtained by considering the actual rooting depth in each slope. Bottom, ADR case: results obtained by considering an arbitrary rooting depth of 1 m in both slopes [Colour figure can be viewed at wileyonlinelibrary.com]

snow pack melt or runoff due to rainfall that exceeds the infiltration capacity of the soil (hortonian runoff), because in these cases the water reaches the stream as surface flow without going into the soil. Computed seasonal evolution of exfiltration flux in SAS and in NAS for both the AC case and the ADR case is shown in Figure 8.

In both cases strong differences between NAS and SAS were seen for the computed exfiltration rates, in terms of both maximum values and seasonal dynamics. The behaviors are also extremely different between the AC and ADR cases, in both the spatial and the temporal location of the maximum fluxes. This again shows the importance of rooting for hydrological processes in the environments considered here. In the AC case, a continuous but small exfiltration flux comes from SAS during the entire active period, while in NAS, exfiltration flux starts only in June, at the beginning of the active layer thaw, and it experiences a strong increase in August when it is more than 50 times higher in NAS than in SAS. This behavior of the AC case is in agreement with field observations.[42,47] By contrast, in the ADR case, there is a strong peak of exfiltration at the beginning of the spring in SAS, while the exfiltrations from SAS and NAS are almost equal at the end of summer.

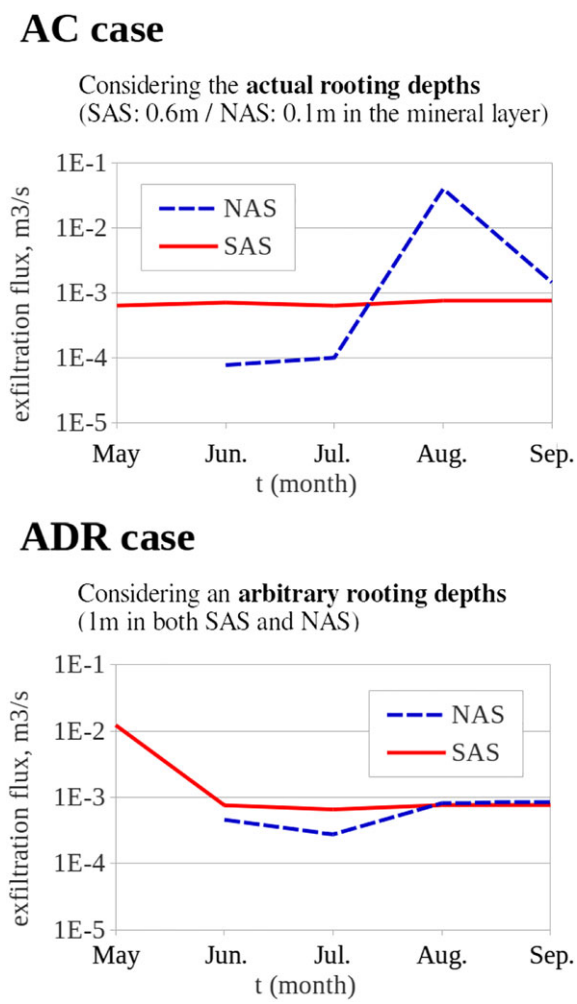

FIGURE 8 Computed seasonal evolution of total exfiltration fluxes from the slopes of the Kulingdakan watershed to the stream. Top, AC case: results obtained by considering the actual rooting depth in each slope. Bottom, ADR case: results obtained by considering an arbitrary rooting depth of 1 m in both slopes [Colour figure can be viewed at wileyonlinelibrary.com]

4 | DISCUSSION

4.1 | Comparison between measured and computed soil temperatures

The mean absolute difference between field measurements and numerical results for soil temperature is lower than 1°C. We thus have a satisfactory agreement as this difference is smaller than the multi-annual standard deviations of the observations (respectively 1.6°C and 2°C for NAS and SAS), and much smaller than the amplitude of the annual variations in soil temperature (20°C for NAS and 22°C for SAS). However, this difference is significant compared to the mean numerical error (~0.05°C) and to the mean error related to the relaxation of the unknown initial conditions (~0.1°C). The associated discrepancies may be due to differences between the real geomorphology of the slopes and the simplified parallelepipedic geometries that are considered for the domains of numerical resolutions and which ignore microtopography, slope variability, and variability of the thickness and nature of the soil horizons. Another possible reason for these differences is the estimate of the thermo-hydrological properties of the soils (see Appendix S2), with no direct field measurement and no calibration. Moreover, we have made the assumption that the horizons are homogeneous in the slopes, thus neglecting, for example, frost cracks and lateral heterogeneities of organic and mineral layer thicknesses along slopes. Finally, another source of error in the numerical results is the use of linearly averaged forcings as input data to model phenomena that are strongly non-linear.

4.2 | Water fluxes: Interpretation of the numerical experiments AC case vs. ADR case

Although there are no field measurements of exfiltration fluxes in the Kulingdakan watershed, the seasonal dynamics of these fluxes have been investigated through quantitative assessment of the temporal variability of the hydrogeochemistry of the catchment waters.[42,47] These observations show that most water input to the stream comes from the NAS, while almost all of the infiltrated waters in SAS are subject to transpiration due to intense evapotranspiration on these slopes.[81] The results in the AC case (the "real" case) are in agreement with these observations, while the results of the ADR case (the "numerical experiment" case) show completely different dynamics, with maximum exfiltration flux at the beginning of spring, and from SAS instead of from NAS. This clearly demonstrates that rooting depth is a key parameter for quantification of the hydrological fluxes in permafrost-dominated forested environments.

As shown by the difference between the maximum active layer thickness computed in the AC case (SAS: 1.41 m; NAS: 0.62 m) and in the ADR case (SAS: 1,1 m; NAS: 0.9 m), the distribution of evapotranspiration uptake in the soil column has a strong impact on the thermal state of the slopes. This is probably mainly due to the important variability of thermal inertia of the soil as a function of its total water content. On the other hand, water may be subject to evapotranspiration only in the thawed soil horizons, and thus there is a complex interplay between evapotranspiration fluxes and active layer

dynamics, due to couplings between water and thermal transfers. In strongly coupled transfer phenomena such as water and thermal transfer in active layers of permafrost, inaccurate estimates of a sink/source term for one equation may have strong impacts on the whole system dynamics, as illustrated here.

Rooting depth is probably of such primary importance for the estimation of actual evapotranspiration because the finer the root layer, the shorter the residence time of infiltrated waters in the evapotranspirative zone. The heterogeneity of the vegetation cover briefly documented in section 2.2.1 then has a major impact on physical processes within the soils of the slopes. Furthermore, the estimated impact would be greater if the variabilities of vegetation morphological parameters other than root depth are also considered. For instance, leaf area index could induce potential evapotranspiration contrasts between slopes.

4.3 | Consequences of identified cryohydrogeological features on weathering processes

Our numerical results confirm that under current conditions, almost no weathering fluxes come from SAS mineral soils, because there are only small water fluxes coming out of SAS. In NAS, the exfiltration fluxes that carry weathering-mobilized matter from the mineral soils occur mostly at the end of summer, but this is only for the upper part of the mineral horizon, as active layer thickness is <0.5 m. Therefore, the present study numerically demonstrates the large impact of permafrost and vegetation cover on water fluxes from soils to the stream previously inferred from biogeochemical observations. The proposed classical theoretical description of transfers in permafrost-dominated, forested areas allows us to reproduce cryohydrogeological dynamics that correlate well with the observed behavior of chemical weathering fluxes.[42,47] Bidimensional variabilites of thermal regimes have been also detected from the numerical results. These differences between upslope and downslope conditions may be related to the fact that soil columns are dryer in the upslope active layer than in the downslope active layer, probably because of supra-permafrost flows that result in lateral transfer of water within the slopes. Lateral transfers have been recently shown to be able to influence permafrost thaw rates.[82,83] These differences in thermal state are likely to generate various local weathering conditions depending on thermal and hydrological heterogeneities within the slopes.

Following a "substituting space for time" approach that is well developed for soils and water in permafrost regions,[84] we may hypothesize that in a warmer climate resulting from global climate change, the hydrobiogeochemical conditions that prevail in NAS will change toward conditions like those that currently prevail in SA. In such a case, weathering fluxes from NAS should decrease substantially, due to decreased water fluxes from soil of these slopes.

Our results confirm that permafrost dynamics and vegetation cover are key factors controlling weathering fluxes from taïga forests under present climatic conditions and ongoing climate change.[6] Overall, the proposed approach of mechanistical modeling of thermo-hydrological behavior of the active layers in the Kulingdakan watershed could provide the basis for assessing the dynamics of the water and element fluxes in forested, permafrost-dominated areas, including changes in weathering processes[85] or the evolution of water stress for tree populations.[86] Moreover, the tool and methodology presented here for the study of the Kulingdakan watershed may, once properly adapted, be usable in other permafrost-affected regions,[87-89] as they do not at any stage require parametrical calibrations, relying on purely mechanistic approaches.

5 | CONCLUSION

To model the thermo-hydrological dynamics of permafrost at time and space scales that are relevant for weathering studies, an OpenFOAM solver for water and energy transfer within variably saturated soils with freeze–thaw of the pore water, the so-called permaFOAM solver, has been developed. PermaFOAM's parallel computing capabilities enabled the modeling of observed annual thermal dynamics of the active layers in a forested watershed with continuous permafrost under current climatic conditions at unprecedentedly fine spatial (2.5 million mesh cells with characteristic lengths from 5 mm to 20 cm) and temporal (from microsecond- to hour-long adaptive time steps) resolutions for several hydrological cycles in a 40-km^2 catchment. Without any parametrical calibration, we obtained reasonably good quantitative agreements between the numerical results and the field data of soil temperature profiles and active layer thicknesses. Furthermore, good qualitative agreement was observed between modeled and real water pathways, as they were characterized by previous hydrobiogeochemical studies of this catchment. Sensitivity analysis highlighted the strong impact of rooting depth on actual evapotranspiration fluxes. This in turn influenced the whole thermo-hydrological dynamics of the active layer, including water fluxes, thermal state and active layer thickness.

Application of this work can first be put to deal with evolution of watershed active layer dynamics under various scenarios of climate change, including to both temperature and atmospheric precipitation. To achieve a predictive modeling under climate change, and to couple climate, snow cover and permafrost dynamics modeling using permaFOAM, we need to model water and energy fluxes within surficial horizons of peat, moss and lichens. Because these media are highly porous, they cannot be properly modeled based on Richards equation, and future works will deal with this specific difficulty.

ACKNOWLEDGEMENTS

We were granted access to the HPC resources of the CALMIP supercomputing center under allocation 2016-[p12166]. We acknowledge support from FCP PHC Campus France (Kolmogorov No. 14.587.21.0036), and from a Russian Science Foundation grant No. 18--17-00237 "Mechanisms of hydrochemical runoff".

ORCID

Laurent Orgogozo https://orcid.org/0000-0001-7752-1427
Anatoly S. Prokushkin https://orcid.org/0000-0001-8721-2142
Oleg S. Pokrovsky https://orcid.org/0000-0002-6440-865X
Christophe Grenier https://orcid.org/0000-0003-4904-3223
Michel Quintard https://orcid.org/0000-0002-6150-7011
Jérôme Viers https://orcid.org/0000-0003-3974-5993
Stéphane Audry https://orcid.org/0000-0002-5075-1262

REFERENCES

1. Grosse G, Goetz S, McGuire AD, Romanovsky VE, Schuur EAG. Changing permafrost in a warming world and feedbacks to the earth system. *Environ Res Lett*. 2016;11(4):040201. https://doi.org/10.1088/1748-9326/11/4/040201
2. Bense VF, Kooi H, Ferguson G, Read T. Permafrost degradation as a control on hydrological regime shifts in a warming climate. *J Geophys Res*. 2012;117:F03036. https://doi.org/10.1029/2011JF002143
3. Walvoord MA, Kurylyk BL. Hydrologic impacts of thawing permafrost a review. *Vadose Zone J*. 2016;15(6). https://doi.org/10.2136/vzj2016.01.0010
4. Wrona FJ, Johansson M, Culp JM, et al. Transitions in arctic ecosystems: ecological implications of a changing hydrological regime. *Eur J Vasc Endovasc Surg*. 2016;121(3):650-674. https://doi.org/10.1002/2015JG003133.
5. Beaulieu E, Goddéris Y, Labat D, Roelandt C, Calmels D, Gaillardet J. Modelling of water-rock interaction in the Mackenzie basin: competition between sulfuric and carbonic acids. *Chem Geol*. 2011;289(1-2):114-123. https://doi.org/10.1016/j.chemgeo.2011.07.020
6. Gooseff MN, McKnight DM, Lyons WB, Blum AE. Weathering reactions and hyporheic exchange controls on stream water chemistry in a glacial meltwater stream in the McMurdo dry valleys. *Water Resour Res*. 2002;38(12):1279-15-17. https://doi.org/10.1029/2001WR000834
7. Zimov SA, Schuur EAG, Chapin FS. Permafrost and the global carbon budget. *Science*. 2006;312(5780):1612-1613. https://doi.org/10.1126/science.1128908
8. Anisimov OA. Potential feedback of thawing permafrost to the global climate system through methane emission. *Environ Res Lett*. 2007;2(4):045016. https://doi.org/10.1088/1748-9326/2/4/045016
9. Kokelj SV, Zajdlik B, Thompson MS. The impacts of thawing permafrost on the chemistry of lakes across the subarctic boreal-tundra transition, Mackenzie Delta region, Canada. *Permafr Periglac Process*. 2009;20(2):185-199.
10. Audry S, Pokrovsky OS, Shirokova LS, Kirpotin SN, Dupré B. Organic matter mineralization and trace element post-depositional redistribution in Western Siberia thermokarst lake sediments. *Biogeosciences*. 2011;8(11):3341-3358. https://doi.org/10.5194/bg-8-3341-2011
11. Shirokova LS, Pokrovsky OS, Kirpotin SN, et al. Biogeochemistry of organic carbon, CO_2, CH_4, and trace elements in thermokarst water bodies in discontinuous permafrost zones of Western Siberia. *Biogeochemistry*. 2013;113(1-3):573-593. https://doi.org/10.1007/s10533-012-9790-4
12. Khvorostyanov DV, Ciais P, Krinner G, Zimov SA. Vulnerability of East Siberia's frozen carbon stores to future warming. *Geophys Res Lett*. 2008;35(10):L10703. https://doi.org/10.1029/2008GL033639
13. Khvorostyanov DV, Ciais P, Krinner G, Zimov SA, Corradi C, Guggenberger G. Vulnerability of permafrost carbon to global warming. Part II: sensitivity of permafrost carbon stock to global warming. *Tellus*. 2008;60B(2):265-275. https://doi.org/10.1111/j.1600-0889.2007.00336.x
14. Guymon GL, Luthin JN. A coupled heat and moisture transport model for arctic soils. *Water Resour Res*. 1974;10(5):995-1001.
15. Kurylyk BL, Watanabe K. The mathematical representation of freezing and thawing processes in variably-saturated, non-deformable soils. *Adv Water Resour*. 2013;60:160-177. https://doi.org/10.1016/j.advwatres.2013.07.016
16. Kurylyk BL, MacQuarrie KTB, McKenzie JM. Climate change impacts on groundwater and soil temperatures in cold and temperate regions: implications, mathematical theory, and emerging simulation tools. *Earth Sci Rev*. 2014;138:313-334. https://doi.org/10.1016/j.earscirev.2014.06.006
17. Vitel M, Rouabhi A, Tijani M, Guérin F. Modelling heat transfer between a freeze pipe and the surrounding ground during artificial ground freezing activities. *Comput Geotech*. 2015;63:99-111. https://doi.org/10.1016/j.compgeo.2014.08.004
18. Holmén J, Benabderrahmane H, Buoro A, Brulhet J. Modelling of permafrost freezing and melting and the impact of a climatic cycle on groundwater flow at the Meuse/haute-Marne site. *Phys Chem Earth*. 2011;36(17-18):1531-1538. https://doi.org/10.1016/j.pce.2011.10.021
19. Grenier C, Régnier D, Mouche E, Benabderrahmane H, Costard F, Davy P. Impact of permafrost development on groundwater flow patterns: a numerical study considering freezing cycles on a two-dimensional vertical cut through a generic river-plain system. *Hydrgeol J*. 2013;21(1):257-270. https://doi.org/10.1007/s10040-012-0909-4
20. Vidstrand P, Follin S, Selroos J-O, Näslund J-O. Groundwater flow modelling of periods with periglacial and glacial climate conditions for the safety assessment of the proposed high-level nuclear waste repository site at Forsmark, Sweden. *Hydrgeol J*. 2014;22(6):1251-1267. https://doi.org/10.1007/s10040-014-1164-7
21. Lemieux JM, Fortier R, Talbot-Poulin MC, et al. Groundwater occurrence in cold environments: examples from Nunavik. *Can Hydrgeol J*. 2016;24(6):1497-1513. https://doi.org/10.1007/s10040-016-1411-1
22. Frampton A, Painter S, Lyon SW, Destouni G. Non-isothermal, three-phase simulations of near-surface flows in a model permafrost system under seasonal variability and climate change. *J Hydrol*. 2011;403(3 4):352-359. https://doi.org/10.1016/j.jhydrol.2011.04.010
23. Zhang J, Qu G, Jin H. Estimates on thermal effects of the China-Russia crude oil pipeline in permafrost regions. *Cold Reg Sci Technol*. 2010;64(3):243-247. https://doi.org/10.1016/j.coldregions.2009.10.001
24. Novikov P, Makarycheva E, Larionov V. Model of permafrost thaw halo formation around a pipeline. In: Lollino G, Giordan D, Thuro K, et al., eds. *Engineering Geology for Society and Territory Volume 6*. Springer International Publishing Switzerland; 2015 https://doi.org/10.1007/978-3-319-09060-3 70.
25. Tan X, Chen W, Tian H, Cao J. Water flow and heat transport including ice/water phase change in porous media: numerical simulation and application. *Cold Reg Sci Technol*. 2011;68(1-2):74-84. https://doi.org/10.1016/j.coldregions.2011.04.004
26. Li G, Yu Q, Ma W, et al. 2015. Freeze-thaw properties and long-term thermal stability of the unprotected tower foundation soils in permafrost regions along the Qinghai-Tibet power transmission line. *Cold Reg Sci Technol*. 2016;121:258-274. https://doi.org/10.1016/j.coldregions.2015.05.004
27. Ghias MS, Therrien R, Molson J, Lemieux J-M. Controls on permafrost thaw in a coupled groundwater-flow and heat-transport system: Iqaluit airport, Nunavut, Canada. *Hydrgeol J*. 2017;25(3):657-673. https://doi.org/10.1007/s10040-016-1515-7
28. Anbergen H, Ruhaak W, Frank J, Sass I. Numerical simulation of a freeze-thaw testing procedure for borehole heat exchanger grouts. *Can Geotech J*. 2015;52(8):1087-1100. https://doi.org/10.1139/cgj-2014-0177
29. Romanovsky VE, Osterkamp TE, Duxbury NS. An evaluation of three numerical models used in simulations of the active layer and permafrost temperature regimes. *Cold Reg Sci Technol*. 1997;26(3):195-203.
30. Painter SL, Moulton JD, Wilson CJ. Modelling challenges for predicting hydrologic response to degrading permafrost. *Hydrgeol J*. 2013;21(1):221-224. https://doi.org/10.1007/s10040-012-0917-4
31. Bierkens MFP, Bell VA, Burek P, et al. Hyper-resolution global hydrological modelling: what is next? "Everywhere and locally relevant". *Hydrol Process*. 2015;29(2):310-320. https://doi.org/10.1002/hyp.10391
32. Karra S, Painter SL, Lichtner PC. Three-phase numerical model for subsurface hydrology in permafrost-affected regions (PFLOTRAN-ICE v1.0). *The Cryosphere*. 2014;8(5):1935-1950. https://doi.org/10.5194/tc-8-1935-2014
33. Painter SL, Coon ET, Atchley AL, et al. Integrated surface/subsurface permafrost thermal hydrology: model formulation and proof-of-concept simulations. *Water Resour Res*. 2016;52(8):6062-6077.
34. Horgue P, Soulaine C, Franc J, Guibert R, Debenest G. An open-source toolbox for multiphase flow in porous media. *Comput Phys Commun*. 2014;187:217-226. https://doi.org/10.1016/j.cpc.2014.10.005

35. Orgogozo L, Renon N, Soulaine C, et al. An open source massively parallel solver for Richards equation: mechanistic modelling of water fluxes at the watershed scale. *Comput Phys Commun*. 2014;185(12):3358-3371. https://doi.org/10.1016/j.cpc.2014.08.004

36. Longshaw SM, Borg MK, Ramisetti SB, et al. mdFoam + : advanced molecular dynamics in OpenFOAM. *Comput Phys Commun*. 2017;224:1-21. https://doi.org/10.1016/j.cpc.2017.09.029.

37. D'Alessandro V, Binci L, Montelpare S, Ricci R. On the development of OpenFOAM solvers based on explicit and implicit high-order Runge Kutta schemes for incompressible flows with heat transfer. *Comput Phys Commun*. 2018;222:14-30.

38. Grenier C, Anbergen H, Bense V, et al. Groundwater flow and heat transport for systems undergoing freeze-thaw: Intercomparison of numerical simulators for 2D test cases. *Adv Water Resour*. 2018;114:196-218. https://doi.org/10.1016/j.advwatres.2018.02.001

39. Pokrovsky OS, Schott J, Kudryavtzev DB. Basalt weathering in Central Siberia under permafrost conditions. *Geochim Cosmochim Acta*. 2005;69(24):5659-5680. https://doi.org/10.1016/j.gca.2005.07.018

40. Pokrovsky OS, Schott J, Dupré B. Trace element fractionation and transport in boreal rivers and soil porewaters of permafrost-dominated basaltic terrain in Central Siberia. *Geochim Cosmochim Acta*. 2006;70(13):3239-3260. https://doi.org/10.1016/j.gca.2006.04.008

41. Bagard M-L, Chabaux F, Pokrovsky OS, et al. Seasonal variability of element fluxes in two central Siberian rivers draining high latitude permafrost dominated areas. *Geochim Cosmochim Acta*. 2011;75(12):3335-3357. https://doi.org/10.1016/j.gca.2011.03.024

42. Bagard M-L, Schmitt A-D, Chabaux F, et al. Biogeochemistry of stable ca and radiogenic Sr isotopes in a larch-covered permafrost-dominated watershed of Central Siberia. *Geochim Cosmochim Acta*. 2013;114:169-187. https://doi.org/10.1016/j.gca.2013.03.038

43. Prokushkin AS, Kajimoto T, Prokushkin SG, McDowell WH, Abaimov AP, Matsura Y. Climatic factors influencing fluxes of dissolved organic carbon from the forest floor in a continuous-permafrost Siberian watershed. *Can J For Res*. 2005;35(9):2130-2140. https://doi.org/10.1139/X05-150

44. Mavromatis V, Prokushkin AS, Pokrovsky OS, Viers J, Korets M. Magnesium isotopes in a permafrost-dominated central Siberian larch forest watersheds. *Geochim Cosmochim Acta*. 2014;147:76-89. https://doi.org/10.1016/j.gca.2014.10.009

45. Price W. Vegetation, microtopography, and depth of active layer on different exposures in subarctic alpine tundra. *Ecology*. 1971;52(4):638-647.

46. Hinkel KM, Nelson FE. Spatial and temporal patterns of active layer thickness at circumpolar active layer monitoring (CALM) sites in northern Alaska, 1995-2000. *J Geophys Res*. 2003;108(D2):8168. https://doi.org/10.1029/2001JD000927

47. Prokushkin AS, Gleixner G, McDowell WH, Ruehlow S, Schulze ED. Source- and substrate-specific export of dissolved organic matter from permafrost-dominated forested watersheds in Central Siberia. *Global Biogeochem Cycles*. 2007;21:GB4003. https://doi.org/10.1029/2007GB002938

48. Orgogozo L. RichardsFOAM2: a new version of RichardsFOAM devoted to the modelling of the vadose zone. *Comput Phys Commun*. 2015;196:619-620. https://doi.org/10.1016/j.cpc.2015.07.009

49. Matsuoka N, Murton J. Frost weathering: recent advances and future directions. *Permafr Periglac Process*. 2008;19(2):195-210. https://doi.org/10.1002/ppp.620

50. Hansson K, Šimůnek J, Mizoguchi M, Lundin L-C, van Genuchten MT. Water flow and heat transport in frozen soil: numerical solution and freeze thaw applications. *Vadose Zone J*. 2004;3:693-704.

51. Painter SL, Karra S. Constitutive model for unfrozen water content in subfreezing unsaturated soils. *Vadose Zone J*. 2014;13(4). https://doi.org/10.2136/vzj2013.04.0071

52. Arzanfudi MM, Al-Khoury R. Freezing-thawing of porous media: an extended finite element approach for soil freezing and thawing. *Adv Water Resour*. 2018;119:210-226. https://doi.org/10.1016/j.advwatres.2018.07.013

53. Zeng Y, Su Z, Wan L, Wen J. A simulation analysis of the advective effect on evaporation using a two-phase heat and mass flow model. *Water Resource Res*. 2011;47:W10529. https://doi.org/10.1029/2011WR010701

54. van Genuchten MT. A closed-form equation for predicting the hydraulic conductivity of unsaturated soils. *Soil Sci Soc Am J*. 1980;44(5):892.

55. McKenzie JM, Voss CI, Siegel DI. Groundwater flow with energy and water-ice phase change: numerical simulations, benchmarks, and application to freezing in peat bogs. *Adv Water Resour*. 2007;30(4):966-983. https://doi.org/10.1016/j.advwatres.2006.08.008

56. Weismüller J, Wollschläger U, Boike J, Pan X, Yu Q, Roth K. Modelling the thermal dynamics of the active layer at two contrasting permafrost sites on Svalbard and on the Tibetan plateau. *The Cryosphere*. 2011;5(3):741-757. https://doi.org/10.5194/tc-5-741-2011

57. Frederick JM, Buffet BA. Taliks in relict submarine permafrost and methane hydrate deposits: pathways for gas escape under present and future conditions. *Case Rep Med*. 2014;119(2):106-122. https://doi.org/10.1002/2013JF002987

58. Kaviany M. *Principles of Heat Transfer in Porous Media*. Second ed. Springer-Verlag New York, Inc; 1995.

59. Liu Z, Yu X. Coupled thermo-hydro-mechanical model for porous materials under frost action: theory and implementation. *Acta Geotechnica*. 2011;6(2):51-65. https://doi.org/10.1007/s11440-011-0135-6

60. Weller HG, Tabor G, Jasak H, Fureby C. A tensorial approach to computational continuum mechanics using object-oriented techniques. *Comput Phys*. 1998;12(6):620-631.

61. Williams GA, Miller CT. An evaluation of temporally adaptive transformation approaches for solving Richards' equation. *Adv Water Resour*. 1999;22(8):831-840.

62. Kurylyk BL, McKenzie JM, MacQuarrie KTB, Voss CI. Analytical solutions for benchmarking cold regions subsurface water flow and energy transport models: one-dimensional soil thaw with conduction and advection. *Adv Water Resour*. 2014;70:172-184.

63. Gentsch N. *Permafrost soils in Central Siberia : landscape controls on soil organic carbon storage in a light taiga biome*. Munich, Germany: Akademische Verlagsgemeinschaft München; 2011.

64. Lebedeva L, Semenova O, Vinogradova T. Simulation of active layer dynamics, upper Kolyma, Russia, using the hydrograph hydrological model. *Permafr Periglac Process*. 2014;25(4):270-280. https://doi.org/10.1002/ppp.1821

65. Prokushkin AS, Hagedorn F, Pokrovsky OS, et al. Permafrost regime affects the nutritional status and productivity of larches in Central Siberia. *Forests*. 2018;9(6):314. https://doi.org/10.3390/f9060314

66. Price JS, Whittington PN, Elrick DE, Strack M, Brunet N, Faux E. A method to determine unsaturated hydraulic conductivity in living and decomposed *Sphagnum* moss. *Soil Sci Soc Am J*. 2008;72(2):487-491. https://doi.org/10.2136/sssaj2007.0111N

67. Voortman BR, Bartholomeus RP, van Bodegom PM, Gooren H, van der Zee SEATM, J-PM W. Unsaturated hydraulic properties of xerophilous mosses: towards implementation of moss covered soils in hydrological models. *Hydrol Process*. 2014;28(26):6251-6264. https://doi.org/10.1002/hyp.10111

68. Szczypta C, Gascoin S, Houet T, et al. Impact of climate and land cover changes on snow cover in a small Pyrenean catchment. *J Hydrol*. 2015;521:84-99. https://doi.org/10.1016/j.jhydrol.2014.11.060

69. Stigter EE, Wanders N, Saloranta TM, Shea JM, Bierkens MFP, Immerzeel WW. Assimilation of snow cover and snow depth into a snow model to estimate snow water equivalent and snowmelt runoff in a Himalayan catchment. *The Cryosphere*. 2017;11(4):1647-1664.

70. Hinkel KM, Outcalt SI, Taylor AE. Seasonal patterns of coupled flow in the active layer at three sites in Northwest North America. *Can J Earth Sci*. 1997;34(5):667-678.

71. Amthor JS, Chen JM, Clein JS, et al. Boreal forest CO_2 exchange and evapotranspiration predicted by nine ecosystem process models: intermodel comparisons and relationships to field measurements. *J Geophys Res*. 2001;106(D24):33623-33648.

72. Lu J, Sun G, McNulty S, Amatya DM. A comparison of six potential evapotranspiration methods for regional use in the southeastern United States. *J Am Water Resour Assoc*. 2005;41(3):621-633.

73. Frolking S. Sensitivity of spruce/moss boreal forest net ecosystem productivity to seasonal anomalies in weather. *J Geophys Res*. 1997;102(24):29053-29064.

74. Romanovsky VE, Drozdov DS, Oberman NG, et al. Thermal state of permafrost in Russia. *Permafr Periglac Process*. 2010;21(2):136-155. https://doi.org/10.1002/ppp.683

75. Farouki OT. Thermal properties of soils. CRREL Monograph 81-1. United States Army Corps of Engineers, Cold Regions Research and Engineering Laboratory, Hanover, New Hampshire, USA. 1981.

76. Wösten JHM, Lilly A, Nemes A, Le Bas C. Development and use of a database of hydraulic properties of European soils. *Geoderma*. 1999;90(3-4):169-185.

77. Duchkov AD, Sokolova LS, Balobaev VT, Devyatkin VN, Kononov VI, Lysak SV. Heat flow and geothermal field in Siberia. *Geologiya / Geofizika*. 1997;38(11):1716-1729.

78. Kollet S, Sulis M, Maxwell RM, et al. The integrated hydrologic model intercomparison project, IH-MIP2: a second set of benchmark results to diagnose integrated hydrology and feedbacks. *Water Resour Res*. 2017;53(1):867-890.

79. Viers J, Prokushkin AS, Pokrovsky OS, et al. Seasonal and spatial variability of elemental concentrations in boreal forest larch foliage of Central Siberia on continuous permafrost. *Biogeochemistry*. 2013;113(1-3):435-449. https://doi.org/10.1007/s10533-012-9770-8

80. Schenk HJ, Jackson RB. The global biogeography of roots. *Ecol Monogr*. 2002;72(3):311-328.

81. Orgogozo L, Pokrovsky OS, Goddéris Y, Viers J, Labat D, Prokushkin A. Numerical modelling of heat and water transfer in permafrost-dominated watersheds. In: Pokrovksy OS, ed. *Permafrost: Distribution, Composition and Impacts on Infrastructure and Ecosystems*. New York, USA: Nova Publishers; 2014:153-172.

82. Kurylyk BL, Hayashi M, Quinton WL, McKenzie JM, Voss CI. Influence of vertical and lateral heat transfer on permafrost thaw, peatland landscape transition, and groundwater flow. *Water Resour Res*. 2016;52(2):1286-1305. https://doi.org/10.1002/2015WR018057

83. Sjölberg Y, Coon E, Sannel ABK, et al. Thermal effects of groundwater flow through subarctic fens: a case study based on field observations and numerical modelling. *Water Resour Res*. 2016;52(3):1591-1606. https://doi.org/10.1002/2015WR017571

84. Raudina TV, Loiko SV, Lim AG, et al. Dissolved organic carbon and major and trace elements in peat porewater of sporadic, discontinuous, and continuous permafrost zones of western Siberia. *Biogeosciences*. 2017;14(14):3561-3584. https://doi.org/10.5194/bg-14-3561-2017

85. Goddéris Y, François LM, Probst A, et al. Modelling weathering processes at the catchment scale: the WITCH numerical model. *Geochim Cosmochim Acta*. 2006;70(5):1128-1147. https://doi.org/10.1016/j.gca.2005.11.018

86. Tchebakova NM, Parfenova EI, Korets MA, Conard SG. Potential change in forest types and stand heights in Central Siberia in a warming climate. *Environ Res Lett*. 2016;11(3):035016. https://doi.org/10.1088/1748-9326/11/3/035016

87. Johansson M, Callaghan TV, Bosiö J, Akerman HJ, Jackowicz-Korczynski M, Christensen TR. Rapid responses of permafrost and vegetation to experimentally increased snow cover in sub-arctic Sweden. *Environ Res Lett*. 2013;8(3):035025. https://doi.org/10.1088/1748-9326/8/3/035025

88. Herod MN, Li T, Pellerin A, Kieser W, Clark ID. The seasonal fluctuations and accumulation of idoine-129 in relation to the hydrogeochemistry of the Wolf Creek Research Basin, a discontinuous permafrost watershed. *Sci Total Environ*. 2016;569-570:121-1223. https://doi.org/10.1016/j.scitotenv.2016.06.196

89. Lindborg T, Rydberg J, Tröjbom M, et al. Biogeochemical data from terrestrial and aquatic ecosystems in a periglacial catchment, West Greenland. *Earth Syst Sci Data*. 2016;8:439-459. https://doi.org/10.5194/essd-8-439-2016